ARTICLES

Aqueous Solutions and Gels of Diblock Copolymers of 1,2-Butylene Oxide and Ethylene Oxide Studied by Light Scattering and Rheology

Antonis Kelarakis, Vasiliki Havredaki, and Kyriakos Viras

National and Kapodiztrian University of Athens, Department of Chemistry, Physical Chemistry Laboratory, Panepistimiopolis, 157 71 Athens, Greece

Withawat Mingvanish, Frank Heatley, and Colin Booth*

Department of Chemistry, University of Manchester, Manchester M13 9PL, U.K.

Shao-Min Mai

Department of Chemistry, University of Sheffield, Sheffield S3 7HF, U.K.

Received: September 18, 2000; In Final Form: April 30, 2001

Copolymers $B_{20}E_{430}$, $B_{20}E_{510}$, and $B_{20}E_{610}$ (B = oxybutylene repeat unit, E = oxyethylene repeat unit, subscripts indicate chain length in repeat units) were synthesized and characterized by gel permeation chromatography (for distribution width) and ^{13}C NMR spectroscopy (for absolute molar mass and composition). Dynamic and static light scattering were used to determine micellar properties in dilute aqueous solution: e.g., micelle association numbers and radii. A tube-inversion method was used to define the mobile−immobile (hard gel) phase boundary. For copolymer $B_{20}E_{610}$, immobile gels form at concentrations as low as 2.9 wt %. Rheological measurements of dynamic modulus and yield stress served to characterize the gel properties and to confirm the phase boundaries. The results are combined with those from previous work on related block copolymers to obtain scaling relationships for the dependence of micellar and gel properties on E-block length, thus enabling prediction of the requirements for and properties of very dilute aqueous gels. The validity of treating the micelles as hard spheres is discussed.

1. Introduction

Block copolyethers in dilute aqueous solution readily form micelles, and their concentrated micellar solutions form liquid-crystal mesophases (gels) comprising packed micelles. From a physicochemical viewpoint, the properties of both are of interest. An account of work on micellar solutions of copolymers of ethylene oxide (EO) and 1,2-butylene oxide (BO) has been published recently,[1] and reviews summarize related work on triblock copolymers of ethylene oxide and propylene oxide.[2,3] A recent paper[4] draws together a considerable body of work on gels of diblock E_mB_n block copolymers. We use the notation E = oxyethylene, OCH_2CH_2, and B = oxybutylene, $OCH_2CH(C_2H_5)$, with m and n denoting block lengths in repeat units.

A recent interest in our laboratory has been the formation and properties of gels of diblock E_mB_n copolymers with long E blocks.[4−6] Copolymers with B blocks in the range $n = 17-19$ and E blocks in the range $m = 96-398$ were prepared and shown to form gels, i.e., spherical micelles packed into cubic structures at concentrations as low as 3.5 wt % in the case of copolymer $E_{398}B_{19}$. These copolymers are referred to hereafter as the B_{18} series. Outside the hard gel region, the micellar solutions of the copolymers exhibited a rich rheological behavior, with well-defined regions of soft gel, i.e., Bingham fluids having yield stress and dynamic storage modulus (G') in excess of loss modulus (G''). We use the terms "hard" and "soft" gel in the manner introduced by Hvidt and co-workers.[7,8] The present work is an extension to copolymers with yet longer E blocks, the aim being to define the E-block length necessary to obtain a cubic-packed hard gel at yet lower concentrations, e.g., 2 wt %. Because it was difficult to mix efficiently a small volume of BO with a large volume of viscous poly(oxyethylene) ($M_n = 20\,000-30\,000$ g mol^{-1}), it was convenient to reverse the sequence of anionic polymerization to BO followed by EO. We denote the copolymers so produced as B_nE_m to signify this change. The series was based on B_{20}, and the copolymers prepared were $B_{20}E_{430}$, $B_{20}E_{510}$, and $B_{20}E_{610}$.

2. Experimental Section

2.1. Copolymers. The diblock copolymers were prepared by sequential anionic polymerization of 1,2-butylene oxide followed by ethylene oxide. The general methods used for their preparation and characterization have been described previously.[9,10] The monofunctional initiator was 2-butanol activated by reaction with potassium metal (mole ratio OH/K ≈ 10). Vacuum line and ampule techniques were used. At the completion of the first

10.1021/jp003364m CCC: $20.00
Published on Web 07/13/2001

TABLE 1: Molecular Characteristics of the Copolymers[a]

copolymer	wt % E (NMR)	$M_n/10^3$ g mol^{-1} (NMR)	M_w/M_n (GPC)	wt % poly(E) (GPC)	$M_w/10^3$ g mol^{-1}
$B_{20}E_{430}$	92.9	20.4	1.06	6	21.6
$B_{20}E_{510}$	94.0	23.9	1.06	8	25.3
$B_{20}E_{610}$	94.9	28.3	1.09	6	30.8

[a] Estimated uncertainties: wt % E to ±0.05; M_n and block lengths to ±3%, M_w/M_n to ±0.02, M_w to ±5%. M_w calculated from M_n and M_w/M_n.

stage, the poly(oxybutylene) precursor was divided between four ampules and dried under vacuum before EO was added.

Characterization of the four copolymers by gel permeation chromatography, GPC, calibrated with poly(oxyethylene) standards, indicated narrow chain length distributions for the copolymers, i.e., $M_w/M_n < 1.10$, where M_w and M_n are the mass-average and number-average molar masses, respectively, plus small shoulders on the low elution volume side attributable to 6-8 wt % poly(oxyethylene) accidentally initiated in the second stage of the polymerization by moisture. Absolute values of M_n of the precursor poly(oxybutylene) and the final copolymers were obtained by ^{13}C NMR spectroscopy by comparison of integrals of resonances from the carbons of end groups, junction groups and backbone groups, based on the assignments of Heatley et al.[11] The spectra also served to confirm the diblock structure and the presence of the poly(oxyethylene) impurity. Relevant molecular characteristics are listed in Table 1, where the formulas are for the copolymer, i.e., corrected for the impurity.

2.2. Light Scattering. Solution clarification and static and dynamic light scattering measurements were carried out as described previously.[5,12] Static light scattering (SLS) intensities were measured by means of a Brookhaven BI 200S instrument using vertically polarized incident light of wavelength $\lambda = 488$ nm supplied by an argon-ion laser (Coherent Innova 90) operated at 500 mW or less. The intensity scale was calibrated against benzene. Dynamic light scattering (DLS) measurements were made under similar conditions, using a Brookhaven BI 9000 AT digital correlator to acquire data. Experiment duration was in the range 5−20 min, and each experiment was repeated two or more times. In both methods, scattered light intensity was usually measured at an angle $\theta = 90°$ to the incident beam.

The correlation functions from dynamic light scattering (DLS) were analyzed by the constrained regularized CONTIN method[13] to obtain distributions of decay rates (Γ), and hence distributions of apparent mutual diffusion coefficient, $D_{app} = \Gamma/q^2$, $q = (4\pi n/\lambda)\sin(\theta/2)$, n is the refractive index of the solvent, and ultimately of apparent hydrodynamic radius ($r_{h,app}$, radius of the hydrodynamically equivalent hard sphere corresponding to D_{app}) via the Stokes−Einstein equation

$$r_{h,app} = kT/(6\pi\eta D_{app}) \quad (1)$$

where k is the Boltzmann constant and η is the viscosity of the solvent at temperature T. In practice, intensities $I(\Gamma)$ delivered by the CONTIN program at logarithmically spaced values of decay rate were transformed to $I(\log \Gamma) = I(\Gamma)\Gamma$ to obtain intensity distributions of $\log(\Gamma)$, and so of $\log(r_{h,app})$. Normalization of $I(\log r_{h,app})$ gave the intensity fraction distributions presented in section 3.1. Average values of Γ, delivered by the CONTIN program by integration over the intensity distributions, were similarly converted to intensity-average values of $r_{h,app.}$ The basis for analysis of static light scattering (SLS) was the Debye equation

$$K^*c/(I - I_s) = 1/M_w + 2A_2c + ... \quad (2)$$

where I is intensity of light scattering from solution relative to that from benzene, I_s is the corresponding quantity for the solvent, c is the concentration (in g dm^{-3}), M_w is the mass-average molar mass of the solute, A_2 is the second virial coefficient (higher coefficients being neglected in eq 2), and K^* is the appropriate optical constant. Values of the specific refractive index increment, dn/dc, its temperature increment, and other quantities necessary for the calculations, have been given previously.[9,12] In fact, values of dn/dc are very similar for poly(oxyethylene) and poly(oxybutylene), making dn/dc insensitive to the exact composition of the copolymers, and making correction for refractive index difference within the copolymer unnecessary.

2.3. Rheometry. The rheological properties of the samples were determined using a Bohlin CS50 rheometer with water-bath temperature control. Couette geometry (bob, 24.5 mm diameter, 27 mm height; cup, 26.5 mm diameter, 29 mm height) was used for all the samples, with 2.5 cm^3 sample being added to the cup in the mobile state. A solvent trap maintained a water-saturated atmosphere around the cell, and evaporation was not significant for the temperatures and time scales investigated.

Storage and loss moduli were recorded across the temperature range with the instrument in oscillatory-shear mode, usually at a frequency of 1 Hz, but for certain systems across the range 0.1−10 Hz. In this mode, the samples were heated at 1 deg min^{-1} in the range 5−92 °C. For all measurements the strain amplitude was low (<0.5%, linear viscoelastic region), thus ensuring that G' and G'' were independent of strain.

Measurements of yield stress and viscosity were made at selected temperatures with the instrument in steady-shear mode. The instrument was programmed to increase the shear stress in a series of logarithmically spaced steps, allowing a maximum of 1 min to equilibrate at each step. Usually, a period of 30 min was allowed for temperature equilibration before starting the program at any given temperature.

In related tube-inversion experiments, samples (0.5 g) were enclosed in small tubes (internal diameter ca. 10 mm) and observed while slowly heating (or cooling) the tube in a water bath, usually within the range 0−70 °C. The change from a mobile to an immobile system (or vice versa) was determined by inverting the tube. The heating/cooling rate was normally 0.5 °C min^{-1}: experiments using a slower heating rate (0.15 °C min^{-1}) gave transition temperatures that differed by less than −1 °C. This simple method of detecting gelation, which is sensitive to the yield stress of the gel, has been shown to define the same hard gel phase boundary as rheometry.[6,14]

3. Micelle Properties by Light Scattering

Solutions of the copolymers did not cloud over the concentration and temperature ranges investigated ($c = 16$ wt %, $T = 90$ °C).

Considering the known effect of B-block length on the critical micelle concentrations of oxyethylene/oxybutylene diblock copolymers,[1,5] it was expected that all three $B_{20}E_m$ copolymers would be completely micellized at room temperature and above. The results obtained for their dilute solutions using dynamic and static light scattering confirmed this, as described below.

3.1. Hydrodynamic Radius. Intensity fraction distributions of apparent hydrodynamic radius [$\log(r_{h,app})$] were obtained by DLS for copolymer solutions at 20, 30, and 40 °C and at concentrations up to 12 g dm^{-3}. The distributions obtained for 1 g dm^{-3} solutions of the three copolymers at 20 °C are shown

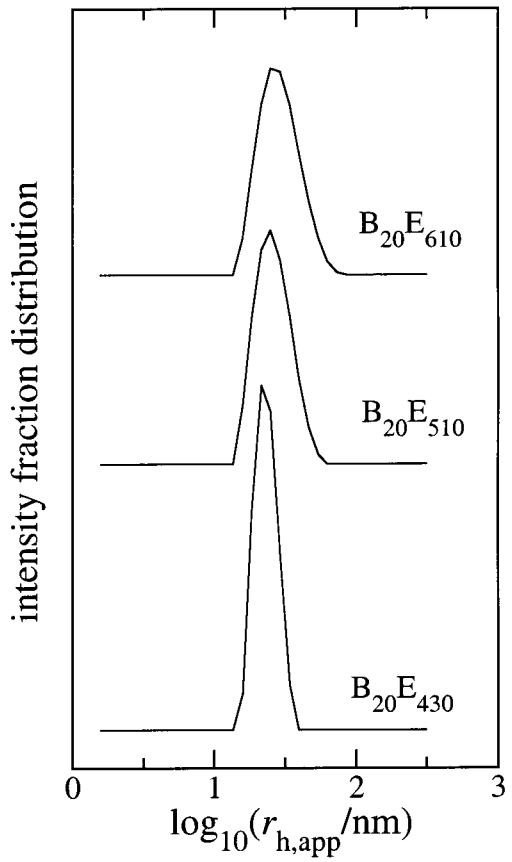

Figure 1. Dynamic light scattering. Intensity fraction distributions of the logarithm of apparent hydrodynamic radius for 1 g dm^{-3} aqueous solutions of $B_{20}E_m$ copolymers at 20 °C, as indicated.

in Figure 1. The single narrow peaks with maxima in the range $r_{h,app} \approx 23-28$ nm indicate micelles formed by closed association. The intensity fraction distributions found at higher concentrations were displaced to lower values of $\log(r_{h,app})$ but were otherwise similar to those shown in Figure 1.

In Figure 2 the reciprocal of the intensity average of $r_{h,app}$ is plotted against copolymer concentration for the three copolymers. Through eq 1, $1/r_{h,app}$ is related to D_{app} but is compensated for change in temperature and viscosity. Complication is avoided in Figure 2 by fitting a single line to all the data points for a given copolymer irrespective of temperature. Linear extrapolation of the individual data sets to zero concentration gave the values of r_h listed in Table 2 (where r_h implies the inverse of the intensity average of $1/r_h$). The positive slope of $1/r_{h,app}$ as a function of c is consistent with spherical micelles effectively interacting as hard spheres. This point is discussed in section 5.2.

The temperature dependence of r_h is small, within the error of determination. It has been known for some time that the hydrodynamic radii of micelles of block copoly(oxyalkylene)s in aqueous solution are insensitive to change in temperature.[1,2] The effect, first noted for $E_mP_nE_m$ copolymers,[15] is attributable to compensation between an increase in association number of the micelle and a decrease in swelling of the micelle fringe as temperature is increased.

3.2. Association Number and Thermodynamic Radius. SLS experiments were performed on copolymer solutions at the temperatures and concentrations described for the DLS experiments. Debye plots, see eq 2 of section 2.2, were used to analyze the data. Used for scattering at 90°, the equation assumes small particles relative to the wavelength of the light. Radii of gyration

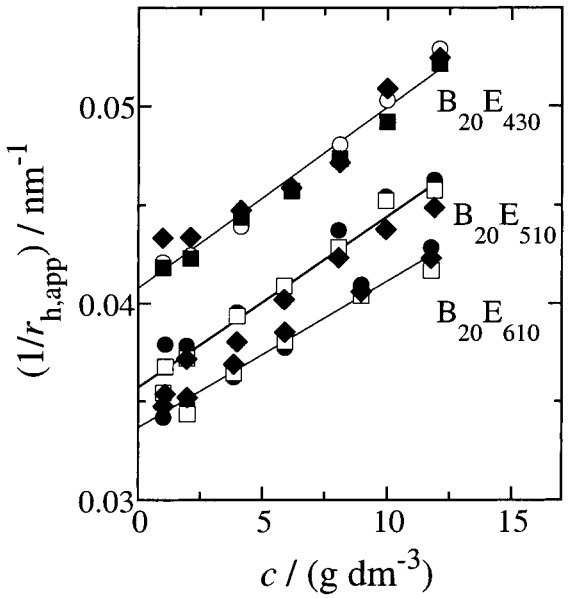

Figure 2. Dynamic light scattering. Concentration dependence of the reciprocal of apparent hydrodynamic radius for aqueous solutions of $B_{20}E_m$ copolymers, as indicated. For each copolymer results are plotted for solutions at 20, 30 and 40 °C.

TABLE 2: Micellar Characteristics from Light Scattering: $B_{20}E_m$ Copolymers in Water[a]

copolymer	T/°C	r_h/nm	$M_w/10^5$ g mol^{-1}	N	δ_t	r_t/nm
$B_{20}E_{430}$	20	25.2	13.5	63	19.4	21.0
	30	24.9	15.5	72	18.7	21.8
	40	24.5	17.4	81	17.8	22.4
$B_{20}E_{510}$	20	27.8	14.3	57	23.0	22.7
	30	28.0	16.8	66	22.5	23.8
	40	28.3	18.4	73	21.4	24.2
$B_{20}E_{610}$	20	30.2	14.6	47	25.7	23.7
	30	30.0	16.8	55	25.0	24.7
	40	29.5	19.1	62	23.3	25.2

[a] r_h (hydrodynamic radius) and r_t (thermodynamic radius), both to ±5%; M_w (mass-average molar mass of micelles), N_w (association number of micelles), and δ_t (thermodynamic expansion factor relative to anhydrous volume), all to ±10%.

estimated as $0.775r_h$ (i.e., as if the micelles were uniform spheres) are in the range 19−23 nm based on the values of r_h listed in Table 2, and a small effect from intraparticle interference is to be expected at the high end of this range. However, from published tables[16] the maximum effect for the largest micelles is to increase M_w by 4%. Given the likely error from other sources, this correction was ignored.

Equation 2 truncated to the second term could not be used in the present experiments because micellar interaction caused significant curvature of the Debye plot even in the low concentration range. This feature is illustrated in Figure 3, in which the reciprocal of the apparent association number, $1/N_{app} = M_{w,mol}K^*c/(I - I_s)$, is plotted against concentration for the three copolymers in solution at 20 °C. This particular plot is preferred for illustrative purposes as the three curves overlap in the usual Debye plot of $K^*c/(I - I_s)$ versus c. Rather than accommodate the curvature by use of a virial expansion, so introducing a number of adjustable coefficients, we have fitted the data with curves based on Perkus−Yevick scattering theory for hard spheres that uses the Carnahan−Starling approximation as proposed by Vrij:[17] see Figure 3. The validity of treating the micelles as hard spheres is discussed in section 5.2. The procedure is equivalent to using the virial expansion for the

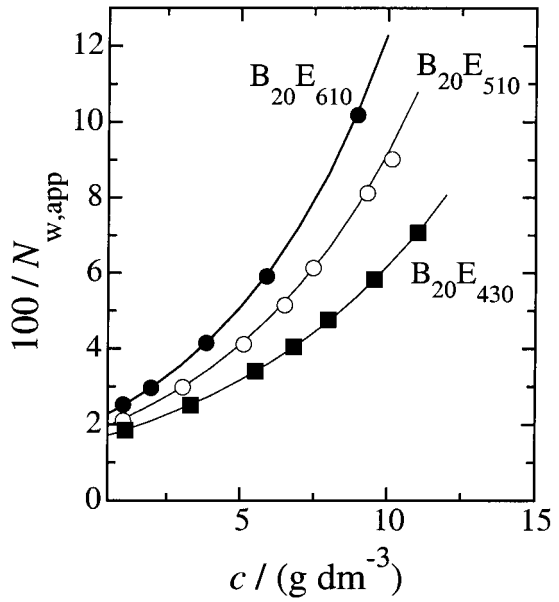

Figure 3. Static light scattering. Concentration dependence of the reciprocal of apparent association number for aqueous solutions of $B_{20}E_m$ copolymers at 20 °C, as indicated.

structure factor for hard spheres taken to its seventh term but requires only two adjustable parameters, M_w and a new parameter, δ_t, related to the volume excluded by one micelle to another, i.e., to the volume fraction occupied by the micelles acting as effective hard spheres. Specifically, δ_t is a thermodynamic expansion parameter defined by where v_t is the

$$\delta_t = v_t/v_a \tag{3}$$

thermodynamic volume (that is one-eighth of the excluded volume for a micelle acting as an effective hard sphere) and v_a is the anhydrous volume of the micelle, i.e.,

$$v_a = M_w/N_A\rho_a \tag{4}$$

where N_A is Avogadro's constant and ρ_a is the density of the copolymers calculated assuming mass additivity of specific volumes from published values for the component homopolymers.[18] Details of the procedure have been described many times previously: see, for example, refs 5, 12, and 19.

Results obtained for the three copolymers at three temperatures are listed in Table 2, together with association numbers of the micelles calculated from

$$N_w = M_{w,mic}/M_{w,mol} \tag{5}$$

using the values of $M_{w,mol}$ listed in Table 1. Also listed is the thermodynamic radius (r_t) calculated from M_w and δ_t via eqs 3 and 4.

4. Gelation and Gel Properties

4.1. Phase Diagrams by Tube Inversion. Mobile−immobile boundaries determined by tube inversion (under the conditions described in section 2.3) are shown in Figure 4. In keeping with previous work on related copolymers,[4−6] and the reports of Hvidt and co-workers,[7,8] the immobile gels are referred to as hard gels. Depending on E-block length, the minimum concentration for hard gel formation (c^*) was in the range 2.9−3.8 wt %, with solutions of copolymer $B_{20}E_{610}$ gelling at the lowest concentrations: see Table 3.

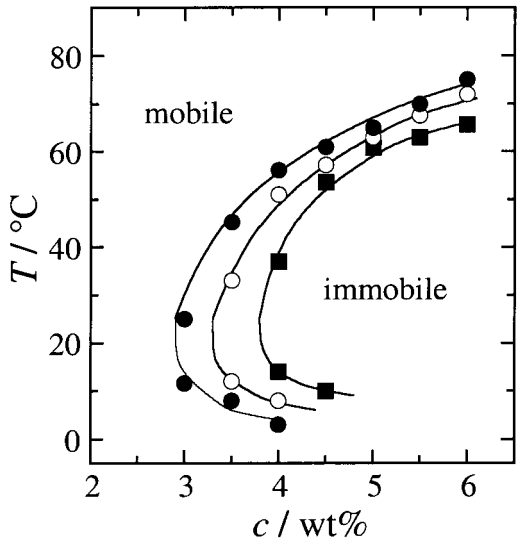

Figure 4. Mobile/immobile boundaries for aqueous solutions of $B_{20}E_m$ block copolymers determined by tube inversion. Results are for (■) $B_{20}E_{430}$, (○) $B_{20}E_{510}$, and (●) $B_{20}E_{610}$. Uncertainty in transition temperatures: ±2 °C.

TABLE 3: Predicted and Observed Values of the Critical Gel Concentration: Micellar Solutions of $B_{20}E_m$ Copolymers at 40 °C

		cgc/wt % at 40 °C	
copolymer	c^*/wt %	predicted	observed
$B_{20}E_{430}$	3.8	4.2	4.0
$B_{20}E_{510}$	3.3	3.5	3.6
$B_{20}E_{610}$	2.9	3.2	3.3

In micellar systems of this type, gelation at any temperature can be understood in terms of solvent-swollen spherical micelles filling space as effective hard spheres.[3,5,7,8,12,20−24] The important parameter is the volume fraction of effective hard spheres. As discussed in section 3.2, the effective size of micelles acting as hard spheres can be derived from the concentration dependence of the intensity of scattered light as the thermodynamic volume v_t, which relates to the volume excluded by one micelle to another. The same quantity is available from other scattering techniques, e.g., small-angle neutron scattering.[19] It is convenient to use the parameter δ_t, and write the volume fraction as

$$\phi = c\delta_t/1000\rho_a \tag{6}$$

where c is the copolymer concentration in g dm^{-3} and ρ_a is the density of anhydrous liquid copolymer as defined in section 3.2. In the particular case of a body-centered cubic (bcc) structure, the critical volume fraction for gelation is $\phi_c = 0.68$, and the critical concentration for hard gel formation (cgc in g dm^{-3}) is

$$\text{cgc}/(\text{g dm}^{-3}) = 680\rho_a/\delta_t \tag{7}$$

Considering solutions at 40 °C, use of eq 7 leads to the predicted values for the cgc (in wt %) that are compared with observed values (interpolated from Figure 4) in Table 3. Prediction and experiment are in good agreement.

4.2. Temperature Dependence of Modulus. *4.2.1. Hard Gels.* As the micellar properties of the present copolymers closely mirrored those reported earlier for the B_{18} series, attention was directed toward the very dilute hard gels formed from copolymer $B_{20}E_{610}$. The effect of concentration and

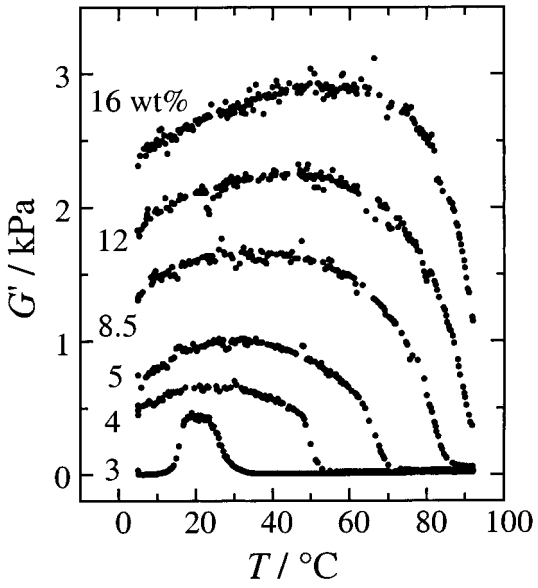

Figure 5. Temperature dependence of storage modulus ($f = 1$ Hz) for aqueous solutions of block copolymer $B_{20}E_{610}$. Copolymer concentrations (wt %) are indicated.

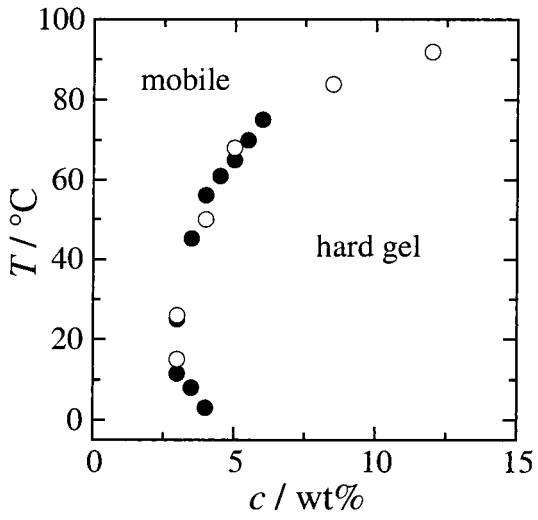

Figure 6. Hard gel phase boundary for aqueous solutions of copolymer $B_{20}E_{610}$ determined either (●) by tube inversion or (○) by rheometry. Uncertainty in transition temperatures: ±2 °C.

temperature on the storage modulus measured at frequency $f =$ 1 Hz is shown in Figure 5. The temperature at which the storage modulus fell steeply to a low value, arbitrarily defined as $G' \approx$ 200 Pa, was used to define the phase boundary. Other realistic choices of G' did not change the temperature by more than ±2 °C. As seen in Figure 6, the phase boundary defined in this way corresponds closely to that defined by tube inversion. In similar experiments carried out at 10 Hz, the hard gel phase boundary was unaffected.

The maximum storage modulus reached by the most dilute hard gel (3 wt %) was only 440 Pa (20 °C, see Figure 5). Nevertheless, the gel remained immobile when held inverted in the tube, indicating a significant yield stress (see section 4.3). However, when subjected to gentle shaking, the gel flowed. A frequency scan for this most dilute solution from 0.1 to 30 Hz (see Figure 7) showed that G' was only weakly dependent on frequency at low values and reached a plateau value at 1 Hz, while G'' fell slightly as the frequency was increased, i.e., behavior somewhat similar to that of a Maxwell element with

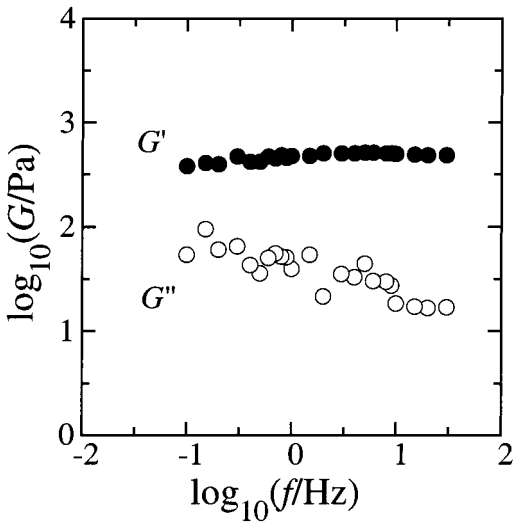

Figure 7. log−log plot showing the frequency dependence of storage and loss modulus for 3.0 wt % aqueous solutions of copolymer $B_{20}E_{610}$ at $T = 20$ °C. Filled symbols denote G' and unfilled symbols denote G''.

a long relaxation time.[25] Dilute hard gels of the other copolymers behaved similarly when tested in this way.

4.2.2. Soft Gels. Examples of plots of log(modulus) against temperature ($f = 1$ Hz) for $B_{20}E_{610}$ solutions are shown in Figure 8. It is seen that the phase transition at high temperature (but not at low, see Figure 8a) is to a fluid with $G' > G''$. As noted in the Introduction, it is convenient to label this fact by calling such mobile fluids soft gels, in contrast to the sols for which $G'' > G'$.

Examples of plots of log(modulus) against temperature ($f =$ 1 Hz) for $B_{20}E_{610}$ solutions below the limiting concentration for hard gel formation are shown in Figure 9. The temperature at which G' obviously exceeds G'' was taken as the lower limit of the soft gel region of the phase diagram under the conditions used. In contrast to the hard gel phase boundary, the temperature of the sol/soft gel boundary decreased on increasing the frequency, much as described previously for micellar solutions of copolymers of the B_{18} series,[6] e.g., by some 20 °C for the 2.5 wt % solution of copolymer $B_{20}E_{610}$ on changing the frequency from 1 to 10 Hz.

A further complication in investigating the soft gels was the time dependence of their properties after loading, i.e., after they had been subject to severe flow. This feature is illustrated in Figure 10 for a 3 wt % solution of copolymer $B_{20}E_{510}$ in its soft-gel phase at 30 °C. The storage modulus measured at $f =$ 1 Hz (see Figure 10a) increased with time from $G' \approx 1$ Pa measured 2 min after loading to $G' \approx 15$ Pa after 68 min, while the loss modulus remained roughly constant. The frequency dependence of storage modulus changed with time after loading (see Figure 10b) from that characteristic of a liquid with a short relaxation time (2 min) to that characteristic of a gel with long relaxation time (68 min). In making the routine measurements described in this paper, about 30 minutes was allowed for equilibration before measurement

The sol/soft-gel boundaries ($f = 1$ Hz) found for dilute solutions of copolymer $B_{20}E_{610}$, and for similarly dilute solutions of copolymers $B_{20}E_{430}$ and $B_{20}E_{510}$, are shown in the combined phase diagram in Figure 11. The straight lines, which highlight the sol/soft gel boundaries, are arbitrarily drawn to meet the hard gel boundaries; the actual behavior at low temperature may well be more complex than that depicted. As would be expected,

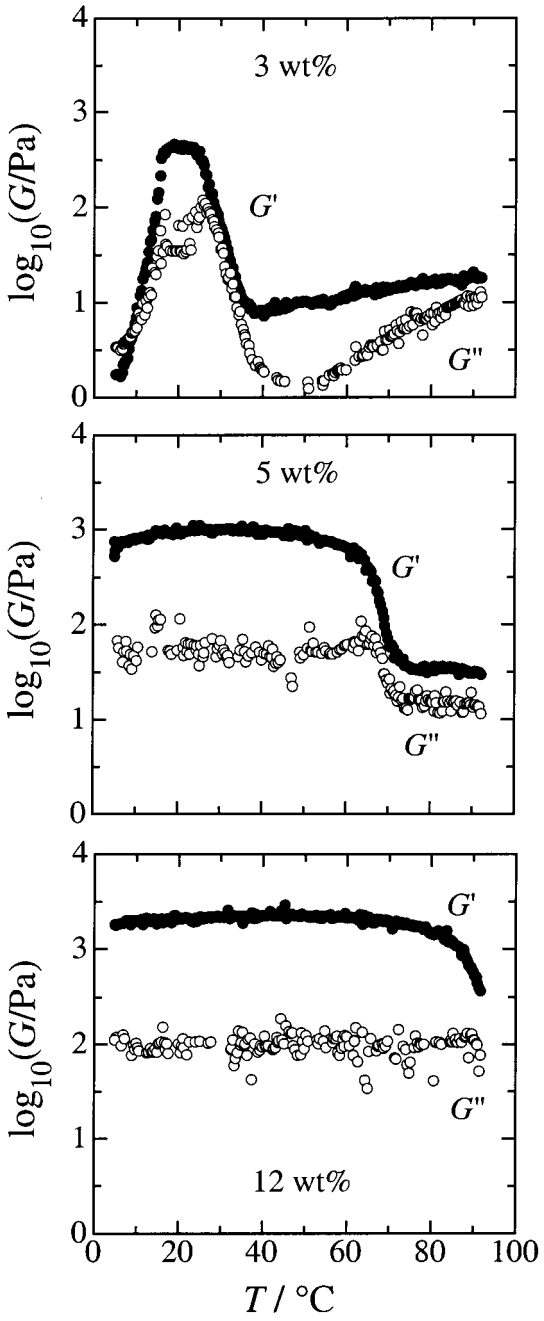

Figure 8. Temperature dependence of logarithmic storage and loss modulus for aqueous solutions of copolymer $B_{20}E_{610}$ at the concentrations (wt %) indicated. Frequency = 1 Hz. Filled symbols denote G' and unfilled symbols denote G''.

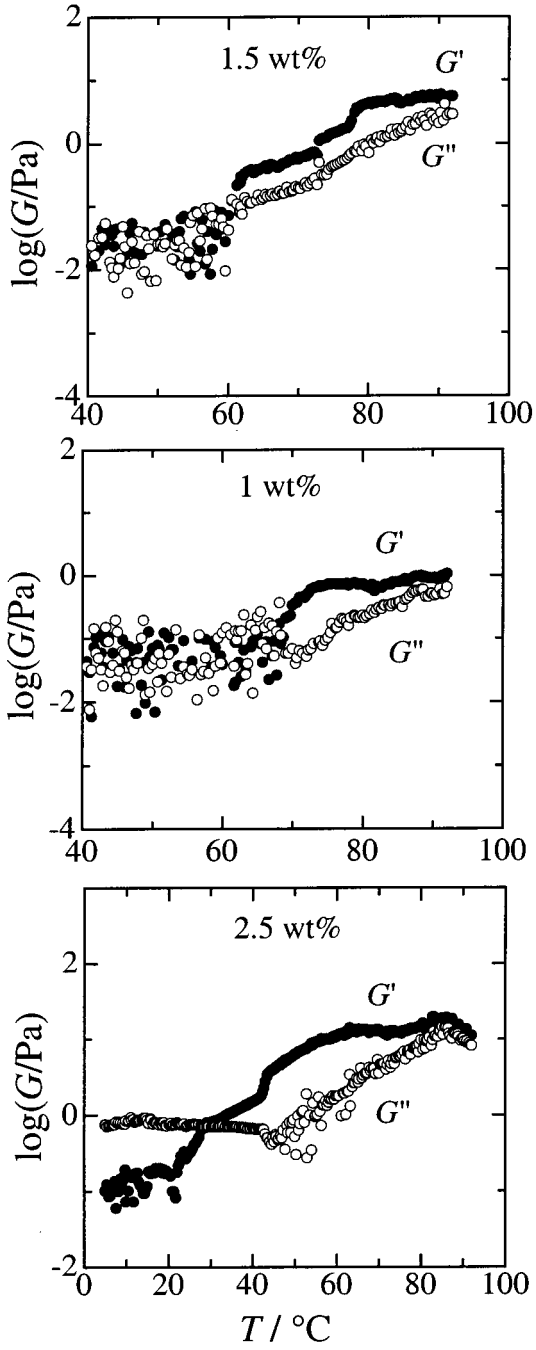

Figure 9. Temperature dependence of logarithmic storage and loss modulus for aqueous solutions of copolymer $B_{20}E_{610}$ at the concentrations (wt %) indicated. Frequency = 1 Hz. Filled symbols denote G' and unfilled symbols denote G''.

the form of this diagram resembles closely that found for dilute solutions of the related copolymers of the B_{18} series (see Figure 9 of ref 6). A similar phase diagram has also been reported for aqueous solutions of a diblock copolymer of ethylene oxide and styrene oxide, $S_{13}E_{60}$.[26]

4.3. Yield Stress. Examples of the effect of a programmed increase in shear stress on micellar solutions of the copolymers are shown in Figure 12 for 3 and 5 wt % solutions of $B_{20}E_{610}$. As indicated in Figure 5, the 3 wt % solution is a sol at low temperature, a hard gel in the interval 15−25 °C, and a soft gel above 30 °C. Figure 12a shows that the sol at 5 °C had zero yield stress, the hard gel at 20 °C had a yield stress of 12 Pa (sufficient to render it immobile in the tube-inversion test provided that it was not shaken), and the soft gel at 35 °C had a low yield stress of 6 Pa. The 5 wt % solution (see Figure 12b) was a stable hard gel at all temperatures below 65 °C, and the yield stresses at 5, 25, and 45 °C were correspondingly high, in the region of 100 Pa. At 65 °C, which is at the boundary between the hard and soft gel (see Figure 5), the yield stress is 5 Pa, characteristic of a soft gel. Other solutions gave similar results: see Table 4. More dilute solutions (3.5 wt % $B_{20}E_{430}$ and 2 wt % $B_{20}E_{610}$) had yield stresses below 2 Pa in their soft gel regions. Parallel to the behavior of the storage modulus, and as noted for the soft gels of the B_{18} series of copolymers,[6] the yield stresses of the soft gels of the present copolymers were reduced to very low values by shearing but recovered after storage for 1 h or more. Given the low levels of yield stress (<2 Pa) found for the dilute gels, and also their shear and time

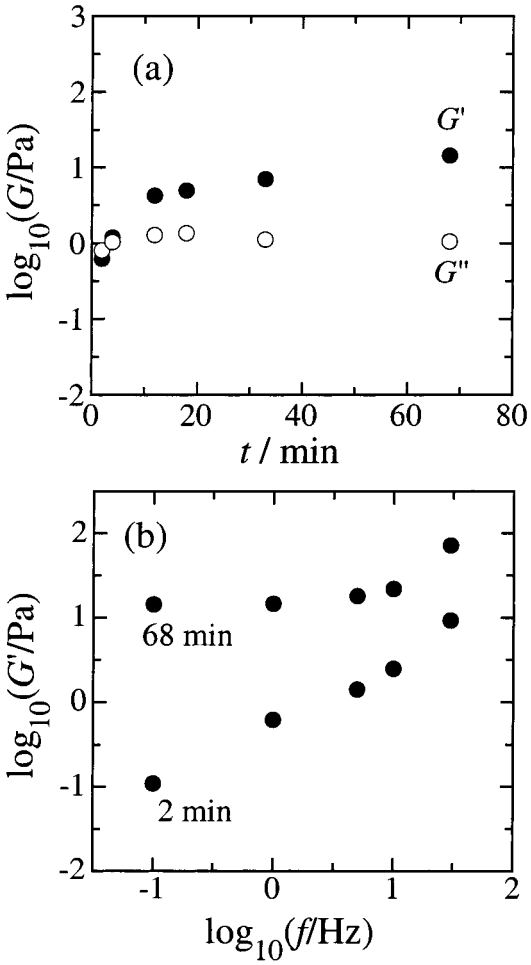

Figure 10. Time dependences in a 3.0 wt % soft gel of copolymer $B_{20}E_{510}$ after flow. $T = 30$ °C. (a) Time dependence of storage and loss modulus measured at frequency 1 Hz. Filled symbols denote G' and unfilled symbols denote G''. (b) Frequency dependence of storage modulus immediately after flow (2 min) and after waiting for 68 min.

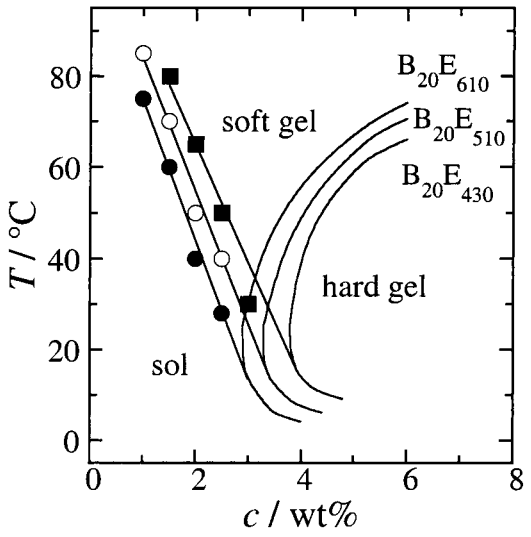

Figure 11. Phase diagram for aqueous solutions of $B_{20}E_m$ block copolymers showing sol, soft gel, and hard gel regions, as indicated. The data points are for soft gels of (■) $B_{20}E_{430}$, (○) $B_{20}E_{510}$, and (●) $B_{20}E_{610}$. The data points omitted from the hard gel boundaries can be seen in Figure 4.

dependence, it was impossible to distinguish soft gel from sol on the basis of yield stress alone. However, as demonstrated in section 4.2.2, the criterion $G' > G''$ held.

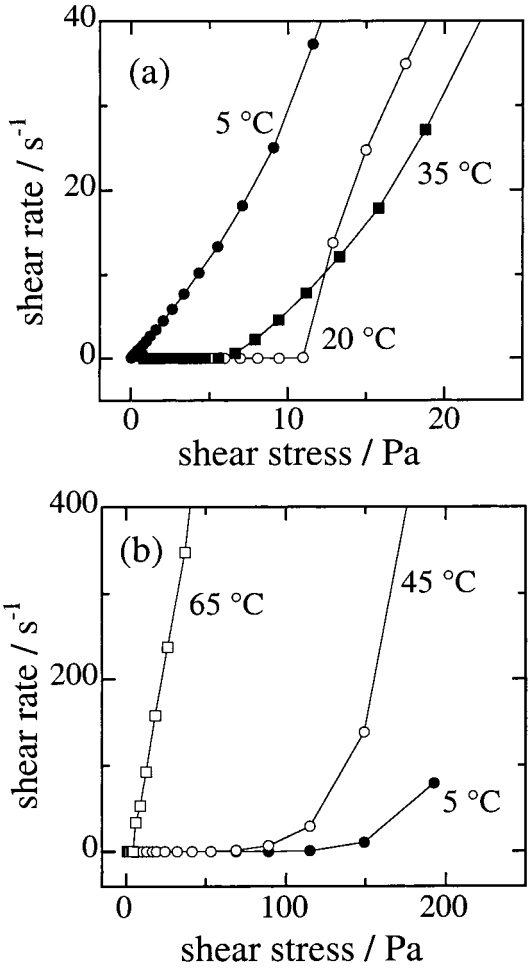

Figure 12. Effect of shear stress on (a) 3 wt % and (b) 5 wt % aqueous gels of copolymer $B_{20}E_{610}$ at the temperatures indicated.

TABLE 4: Yield Stresses (σ_y/Pa) of Aqueous Solutions of $B_{20}E_m$ Block Copolymers

	$B_{20}E_{610}$			$B_{20}E_{430}$
T/°C	3 wt %	5 wt %	10 wt %	4 wt %
5	0	110[a]	340[a]	22[b]
15	8			37[b]
20	12[a]			
25	8	130[a]	220[a]	29[b]
35	7			10
45	6	80[a]	220[a]	2
65		5	120[a]	2
85		7	5	3

[a] Denotes immobile gel in the tube-inversion test. [b] Not investigated by tube inversion.

5. Effect of E Block Length: Comparison of Present and Previous Results

5.1. Micelle Association Number and Radius. From Table 2, it is apparent that values of the radii increase with increase in E-block length while values of the micelle association number decrease. This is illustrated in the log−log plots of Figure 13, where the present results for the $B_{20}E_m$ copolymers in solution at 40 °C are compared with those obtained previously[5] under the same conditions for the four E_mB_n block copolymers of the B_{18} series. The straight lines in Figure 13, which are drawn through the combined data points for both series, emphasize the agreement between the data sets. The apparent insensitivity of micellar properties to B-block length is unexpected in view

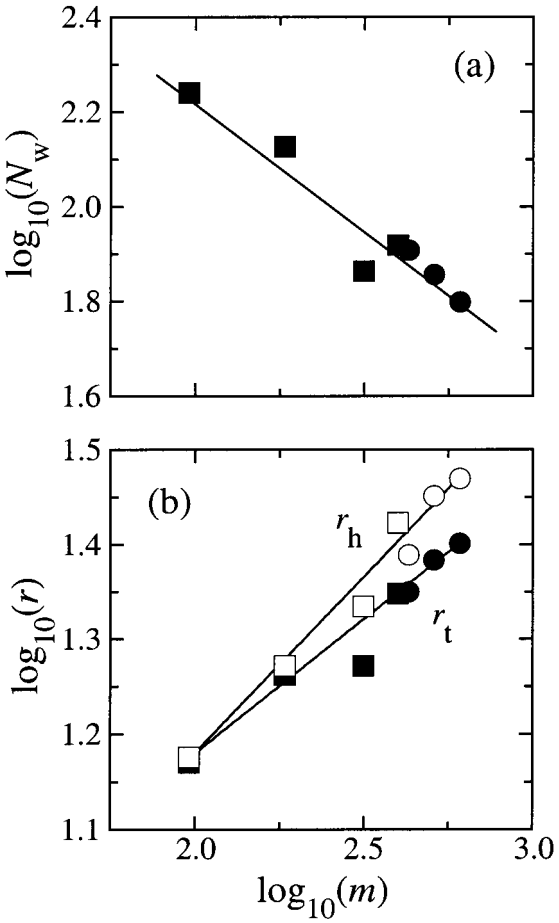

Figure 13. (a) log−log plot of mass-average association number versus E-block length for micelles of (●) $B_{20}E_m$ and (■) E_mB_{18} block copolymers in aqueous solution at 40 °C. (b) log−log plots of micelle radius versus E-block length for micelles of the same block copolymers. Filled symbols denote the thermodynamic radius (r_t) and unfilled symbols the hydrodynamic radius (r_h).

of the many results indicating otherwise.[1] Possibly, it is a consequence of the difference in the order of polymerization (BE versus EB), which means that the B blocks in the B_nE_m copolymers terminate in methyl groups whereas those in the E_mB_n copolymers terminate in hydroxyl groups. This possibility will be investigated in the near future.

In Figure 13a, the slope of the best straight line through the combined points corresponds to

$$N_w \sim m^{-0.55\pm0.07}$$

which is in agreement with the exponent −0.51 derived theoretically for E_mP_n diblock copolymers by Nagarajan and Ganesh.[27] This is an equilibrium treatment based on the Flory−Huggins model in which the water/polymer interactions are introduced via known values of parameter χ for water/poly(oxyethylene) and water/poly(oxypropylene). The scaling exponent of $m^{-0.51}$ is system specific but depends essentially on the fact that water at low temperatures is a good solvent for poly(oxyethylene). Accordingly, one might reasonably expect similar behavior for the two systems, E_mP_n and E_mB_n, which both have poly(oxyethylene) coronal blocks.

As reviewed by Hamley,[28] and discussed previously in relation to related copolymers,[1,20] theoretically derived scaling laws for micelle radius of gyration (or the micelle corona thickness, which is a large part of the micelle radius in the present systems), place the exponent of m in the range 0.5−0.8. Of the two radii measured in the present work, the hydrodynamic radius is most closely related to those considered by theory, but the exponent obtained from the combined plot in Figure 13b ($r_h \sim m^{0.37\pm0.04}$) lies outside the range of predicted values. This value, and the corresponding exponent for the thermodynamic radius ($r_t \sim m^{0.28\pm0.03}$), are similar to values reported previously for related block copolymers.[20]

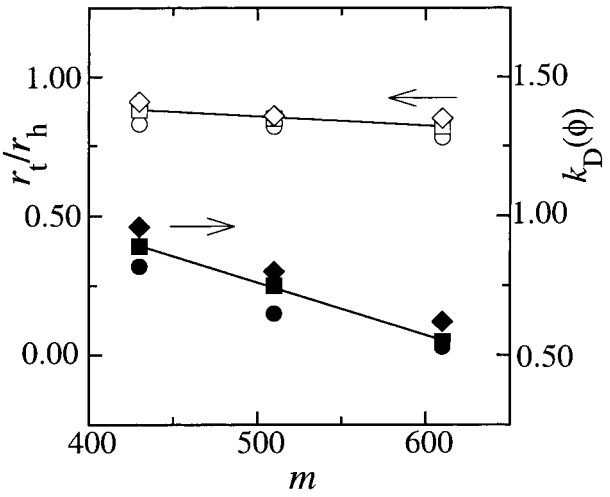

Figure 14. Dependence on E-block length (m, $B_{20}E_m$ copolymers) of the ratio of micelle thermodynamic and hydrodynamic radii (r_t/r_h, left-hand axis, unfilled symbols) and of the diffusion virial coefficient ($k_D(\phi)$, right-hand axis, filled symbols). The data points are for (○, ●) 20 °C, (□, ■) 30 °C, and (◇, ◆) 40 °C.

5.2. $B_{20}E_m$ Micelles as Hard Spheres. A combination of dynamic and static light scattering enables investigation of the validity of considering the micelles as hard spheres. One approach is to compare directly the values of the effective hard-sphere radii arising from the two methods, as the ratio r_t/r_h should be unity for a completely hard sphere. As reviewed by Selser,[29] this parameter is used in investigating the nature of the coil−coil interaction of polymers in solution. Values of the ratio are plotted against E-block length in Figure 14 and are seen to be below unity, especially for the copolymer with the longest E blocks, which is consistent with the most expanded corona giving the softest interaction potential. We have shown previously that micelles of comparable copolymers with significantly shorter E blocks have r_t/r_h closer to unity, e.g., 0.93 for $E_{96}B_{18}$ in aqueous solution at 20 °C,[4] As the temperature is raised, the solvent becomes poorer, resulting in an increase in micellar association number (Table 2). This counteracts the expected increase in interpenetration of the E blocks in the corona of the micelle (i.e., a softening of the interaction potential), and the overall effect is an increase in r_t/r_h: see Figure 14. This complication is, of course, peculiar to associating systems.

In a related approach, applied to micelles by Konak et al.,[30] the second diffusion virial coefficient (k_D) obtained from a plot of the apparent diffusion coefficient against c, i.e.

$$D_{app} = D(1 + k_D c)$$

is expressed in volume fraction units as

$$k_D(\phi) = k_D/\bar{v} \approx k_D m_w/v_h$$

where $\bar{v}$ is the partial specific volume and m_w and v_h are respectively the average mass ($m_w = M_w/N_A$) and hydrodynamic

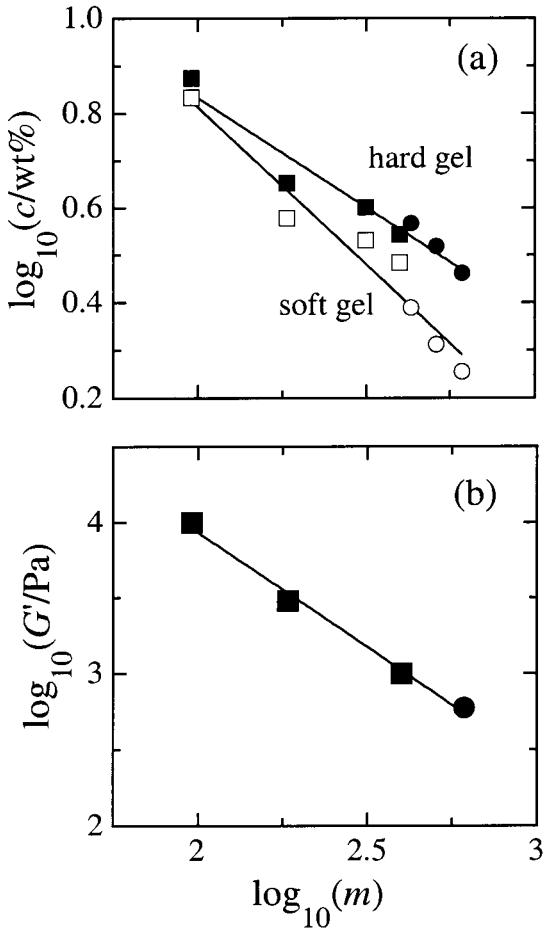

Figure 15. (a) log−log plot of the concentration of gel formation versus E-block length for micellar solutions of (●, ○) $B_{20}E_m$ and (■, □) E_mB_{18} block copolymers in aqueous solution. Filled symbols denote the minimum concentration for hard gel formation (c^*); unfilled symbols denote the concentration for soft gel formation at 50 °C and 1 Hz (c^{**}). (b) log−log plots of storage modulus versus E-block length for micellar solutions of the same block copolymers. The storage modulus plotted is the maximum value measured for a solution of concentration $c \approx c^* + 1$ wt % during a temperature sweep at $f = 1$ Hz.

volume [$v_h = (4\pi/3)r_h^3$] of the micelles. As can be inferred from Figure 2, values of k_D are readily obtained from linear fits of $D_{app}(c)$. Values of $k_D(\phi)$ derived by making use of the micellar properties in Table 2 are plotted against E-block length in Figure 14. Because the two parameters are closely related,[29] the dependences of $k_D(\phi)$ on E-block length and temperature follow those of r_t/r_h. A realistic criterion for approximate hard sphere behavior, matching $r_t/r_h \rightarrow 1$, is $k_D(\phi) \geq 2$. On the other hand, the soft sphere behavior of polymer coils in poor solvents is characterized by $r_t/r_h \rightarrow 0$ (approaching the theta condition) and $k_D(\phi) \leq -2$. Taking these results into account, the micelles of the $B_{20}E_m$ copolymers may be considered as moderately hard, making it reasonable to treat them as hard spheres in the analysis of static light scattering data.

5.3. Gel Formation and Storage Modulus. The log−log plot in Figure 15a shows the dependence on E-block length of the minimum concentration for hard gel formation (c^*) for the copolymers of the B_{20} and B_{18} series. The combined data scale as

$$c^* \sim m^{-0.46\pm0.05}$$

allowing the prediction that formation of a 2 wt % aqueous hard gel would require synthesis (within the present series) of a micellizable $B_{20}E_{1300}$ copolymer.

The storage modulus of the hard gel can be similarly related to E-block length. In this case consideration has to be given to the choice of gel concentration at which G' is measured. As demonstrated previously,[6] concentrations equivalently displaced from c^* are satisfactory for this purpose, and the modulus considered here is the maximum value measured for a solution of concentration $c \approx c^* + 1$ wt % during a temperature sweep at $f = 1$ Hz: see, for example, Figure 5, $c = 4$ wt %. The resulting log−log plot of G' against E-block length, shown in Figure 15b, leads to

$$G' \sim m^{-1.52\pm0.09}$$

and to the prediction that a 3 wt % aqueous gel of copolymer $B_{20}E_{1300}$ would have a storage modulus of ca. 200 Pa, and a correspondingly low yield stress. Probably this gel would flow in the tube-inversion test used in this work and a more sensitive tube test, for example, that described by Hvidt et al.,[7] might be required to define its phase boundary. However, the important characteristics of the hard gel phase should be retained, certainly the ordered cubic packing and probably the frequency-independent storage modulus.

Considering the soft gels, there is no obvious concentration on which to base a plot parallel to c^* for the hard gels. The concentration at the sol/soft-gel boundary (c^{**}) depends on choice of temperature and frequency. The formation of soft gels of this type has been ascribed to a percolation mechanism whereby structures of weakly interacting spherical micelles form in the system. The transition from sol to soft gel is assumed to occur when micellar aggregates reach a percolation threshold yielding sufficient structure to cause an increase in modulus and, at a suitable frequency, the dynamic storage modulus to exceed the loss modulus.[6,26,31,32] As noted previously,[6] it will be necessary to understand the frequency dependence of the sol/soft-gel transition and to confirm the presence of fractal micellar aggregates. For the present, it is noted that a log−log plot of c^{**} measured at 50 °C and 1 Hz (see Figure 14a) gives a straight line conforming to the relation $c^{**} \sim m^{-0.67\pm0.07}$.

6. Concluding Remarks

The dependence of the micellar properties (i.e., association number and radius) of E/B diblock copolymers on E-block length has been investigated for copolymers with E-block lengths up to E_{610}. The behavior is as expected, i.e., related to that of their analogues with shorter chain lengths. The same is true of gelation concentration and gel properties (e.g., modulus), which is a direct consequence of the fact that these properties depend on micelle properties. The scaling relations obtained allow secure prediction of the synthetic requirements for the preparation of extremely dilute aqueous packed gels: for example, formation of a 2 wt % aqueous gel will require synthesis of a micellizable E/B copolymer with an E-block length of ca. 1300 chain units. Parallel scaling relationships enable prediction of gel properties.

Acknowledgment. We thank Mr. S. K. Nixon and Miss C. Chaibundit for help with the copolymer characterization. Financial support was provided by the Thai Government (for W.M.) and the Erasmus Exchange Program of the European Union (for A.K.). The Engineering and Physical Research Council (UK) supported the synthesis of block copolymers through grant GR/L22645.

References and Notes

(1) Booth, C.; Attwood, D *Macromol. Rapid Commun.* **2000**, *21*, 501.

(2) Chu, B.; Zhou, Z.-K. In *Nonionic Surfactants: Polyoxyalkylene Block Copolymers*; Nace, V. M., Ed.; Marcel Dekker: New York, 1996; Chapter 3.

(3) Mortensen, K. In *Amphiphilic Block Copolymers: Self-assembly and Applications*; Alexandridis, P., Lindman, B., Ed.; Elsevier Science B.V: Amsterdam, 2000, Chapter 9.

(4) Hamley, I. W.; Daniel, C.; Mingvanish, W.; Mai, S.-M.; Booth, C.; Messe, L.; Ryan, A. J. *Langmuir* **2000**, *16*, 2508.

(5) Mingvanish, W.; Mai, S.-M.; Heatley, F.; Booth, C.; Attwood, D. *J. Phys. Chem. B* **1999**, *103*, 11269.

(6) Kelarakis, A.; Mingvanish, W.; Daniel, C.; Li, H.; Havredaki, V.; Booth, C.; Hamley, I. W.; Ryan, A. J. *Phys. Chem. Chem. Phys.* **2000**, *2*, 2755.

(7) Hvidt, S.; Jørgensen, E. B.; Brown, W.; Schillen, K. *J. Phys. Chem.* **1994**, *98*, 12320.

(8) Almgren, M.; Brown, W.; Hvidt, S. *Colloid Polym. Sci.* **1995**, *273*, 2.

(9) Bedells, A. D.; Arafeh, R. M.; Yang, Z.; Attwood, D.; Heatley, F.; Padget, J. C.; Price, C.; Booth, C. *J. Chem. Soc., Faraday Trans.* **1993**, *89*, 1235.

(10) Yu, G.-E.; Yang, Z.; Ameri, M.; Attwood, D.; Collett, J. H.; Price, C.; Booth, C. *J. Phys. Chem., Part B* **1997**, *101*, 4394.

(11) Heatley, F.; Yu, G.-E.; Sun., W.-B.; Pywell, E. J.; Mobbs, R. H.; Booth, C. *Eur. Polym. J.* **1990**, *26*, 583.

(12) Deng, N.-J.; Luo, Y.-Z.; Tanodekaew, S.; Bingham, N.; Attwood, D.; Booth, C. *J. Polym. Sci., Part B, Polym. Phys.* **1995**, *33*, 1085.

(13) Provencher, S. W. *Makromol. Chem.* **1979**, *180*, 201.

(14) Li, H.; Yu., G.-E.; Price, C.; Booth, C.; Hecht, E.; Hoffmann, H. *Macromolecules* **1997**, *30*, 1347.

(15) Attwood, D.; Collett, J. H.; Tait, C. J. *Int. J. Pharm.* **1985**, *26*, 25.

(16) Casassa, E. F. In *Polymer Handbook*, 3rd ed.; Brandrup, J., Immergut, E. H., Eds.; Wiley: New York, 1989; p 485. Beattie, W. H.; Booth, C. *J. Phys. Chem.* **1960**, *64*, 696.

(17) Percus, J. K.; Yevick, G. J. *J. Phys. Rev.* **1958**, *110*, 1. Vrij, A. *J. Chem. Phys.* **1978**, *69*, 1742. Carnahan, N. F.; Starling, K. E. *J. Chem. Phys.* **1969**, *51*, 635.

(18) Mai, S.-M.; Booth, C.; Nace, V. M. *Eur. Polym. J.* **1997**, *33*, 991.

(19) Derici, L.; Ledger, S.; Mai, S.-M.; Booth, C.; Hamley, I. W.; Pedersen, J. S. *Phys. Chem. Chem. Phys.* **1999**, *1*, 2773.

(20) Chaibundit, C.; Mai, S.-M.; Heatley, F.; Booth, C. *Langmuir* **2000**, *16*, 9645.

(21) Wanka, G.; Hoffmann, H.; Ulbricht, W. *Macromolecules* **1994**, *27*, 4145.

(22) Mortensen, K.; Brown, W. *Macromolecules* **1993**, *26*, 4128. Mortensen, K.; Pedersen, J. S. *Macromolecules* **1993**, *26*, 805.

(23) Malmsten, M.; Lindman, B. *Macromolecules* **1992**, *25*, 5440.

(24) Bedells, A. D.; Arafeh, R. M.; Yang, Z.; Attwood, D.; Padget, J. C.; Price, C.; Booth, C. *J. Chem. Soc., Faraday Trans.* **1993**, *89*, 1243.

(25) J. D. Ferry, *Viscoelastic Properties of Polymers*; Wiley: New York, 1961; Chapter 3.

(26) Kelarakis, A.; Havredaki, V.; Rekatas, C.; Mai, S.-M.; Attwood, D.; Booth, C.; Ryan, A. J.; Hamley, I. W.; Martini, L. G. A. *Macromol. Chem. Phys.* **2001**, *202*, 1345.

(27) Nagarajan, R.; Ganesh, K. *J. Chem. Phys.* **1989**, *90*, 5843.

(28) Hamley, I. W. *The Physics of Block Copolymers*; Oxford University Press: Oxford, U.K., 1998; pp 163−174

(29) Selser, J. In *Light Scattering: Principles and Development*; Brown, W., Ed.; Clarendon Press: Oxford, U.K., 1996; Chapter 7.

(30) Konak, C.; Tuzar, Z.; Stepanek, P.; Sedlacek, B.; Kratochvil, P. *Prog. Colloid Polym. Sci.* **1985**, *71*, 15.

(31) Lobry, L.; Micali, N.; Mallamace, F.; Liao, C.; Chen, S.-H. *Phys. Rev. E* **1999,** *60*, 7076.

(32) Winter, H. H.; Mours, M. *Adv. Polym. Sci.* **1997**, *134*, 165.